Ionic Effects in Collapse of Polyelectrolyte Brushes

Tao Jiang and Jianzhong Wu*

Department of Chemical and Environmental Engineering, University of California, Riverside, California 92521-0444

Received: March 4, 2008

We investigated the effect of counterion valence on the structure and swelling behavior of polyelectrolyte brushes using a nonlocal density functional theory that accounts for the excluded-volume effects of all ionic species and intrachain and electrostatic correlations. It was shown that charge correlation in the presence of multivalent counterions results in collapse of a polyelectrolyte brush at an intermediate polyion grafting density. At high grafting density, the brush reswells in a way similar to that in a monovalent ionic solution. In the presence of multivalent counterions, the nonmonotonic swelling of a polyelectrolyte brush in response to the increase of the grafting density can be attributed to a competition of the counterion-mediated electrostatic attraction between polyions with the excluded-volume effect of all ionic species. While a polyelectrolyte brush exhibits an "osmotic brush" regime at low salt concentration and a "salted brush" regime at high salt concentration regardless of the counterion valence, we found a smoother transition as the valence of the counterions increases. As observed in recent experiments, a quasi-power-law dependence of the brush thickness on the concentration ratio can be identified when the monovalent counterions are replaced with trivalent counterions at a fixed ionic strength.

Introduction

In a highly charged polyelectrolyte system, the presence of multivalent counterions may result in counterintuitive electrostatic phenomena such as attraction between like charges and charge inversion that defy predictions of conventional mean-field theories. For example, a mean-field approach based on the Poisson−Boltzmann theory would predict that like-charged polyelectrolytes will always repel each other.[1] However, many experiements,[2–7] simulations,[8–13] and theoretical calculations[14–19] all indicate that the electrostatic interaction between like-charged polyelectrolytes can be attractive if they are surrounded by multivalent counterions (i.e., monomeric ionic species of opposite charge). The counterion-mediated electrostatic attraction may lead to drastic conformational changes of the polyelectrolyte chains and various macroscopic or mesoscopic phase transitions in polyelectrolyte systems.[9,20]

Polyelectrolyte brush (PEB) represents a unique polyelectrolyte system where each chain (polyion) is end-grafted to a surface or an interface by chemical or physical means.[21–23] Because of the tethering effect, the properties of a PEB can be quite different from those corresponding to free polyelectrolytes in an aqueous solution. Nevertheless, the counterion valence plays a pivotal role in determining the properties of a PEB just as that in its bulk solution counterparts. As one may expect on the basis of mean-field predictions, the electrostatic interaction between grafted polyelectrolytes is always repulsive in a solution with only monovalent counterions. As a result, a PEB swells monotonically as the grafting density increases and collapses in a salt solution. The swelling of a PEB in the presence of monovalent counterions has been extensively reported and can be successfully described by various mean-field theories and scaling analysis.[24–29]

An increase of the counterion valence from monovalent to trivalent results in qualitative differences in the swelling behavior.[30–33] In a solution containing only monovalent counterions, the brush thickness increases monotonically with the polyelectrolyte graft density at a given salt concentration. By contrast, molecular simulation for a PEB of rodlike polyions indicates that the thickness of a PEB may decline with the increase of grafting density in a solution containing multivalent counterions.[33] Additionally, the counterion valence also affects the distributions of polyion segments and counterions within the brush. Although the polymer model used in this simulation is probably oversimplified, we expect that similar conclusions are valid for realistic PEBs.

In contrast with predictions of a typical mean-field theory, at the same ionic strength or the Debye screening length, a PEB swells in a monovalent solution but collapses if the counterions are replaced with multivalent ones. For example, it was shown experimentally that replacement of Na^+ with La^{3+} at the fixed ionic strength results in collapse of polystyrene sulfonic acid brush tethered on spherical particles.[31] Similarly, the conformation of a star polyelectrolyte can be reversibly manipulated by changing the valence of counterions.[32] In a solution with divalent or trivalent counterions, the size of star polyelectrolytes is drastically reduced in comparison with that in a monovalent solution. The conformation can be restored by removing the multivalent ions. In light of attraction between similar charges in a solution with multivalent ions, one may argue that the collapse of a PEB can be attributed to counterion-mediated electrostatic attraction among polyions. However, van der Waals attraction and solvent-mediated forces are ubiquitous in experimental systems. A direct linkage between electrostatic correlations and the nonmonotonic swelling behavior of a PEB in a multivalent solution is not immediately obvious.

Recently, we investigated the properties of PEBs using the primitive model where both polyion segments and monomeric ions are represented by charged hard spheres and the solvent is represented by a dielectric continuum.[34,35] To confine our interest to charge correlations, we deliberately avoid the van der Waals attraction among all ionic species, which may be significant in

* To whom correspondence should be addressed. E-mail: jwu@engr.ucr.edu.

10.1021/jp801911a CCC: $40.75
Published on Web 06/11/2008

realistic polyelectrolyte systems.[36] Using a nonlocal density functional theory (DFT) that accounts for the excluded-volume effects of all ionic species, intrachain correlations, and electrostatic correlations,[37,38] we found that the primitive model is able to capture the effects of salt concentration, polyion grafting density, and chain length on the swelling and structures of the PEB all in good agreement with simulation or experimental results.[34] At low salt concentration, the DFT predicts that multivalent counterions may self-organize into a wavelike structure in a highly charged PEB, resembling the wavelike distribution of ions between Actin fibers in an aqueous environment. The ion-mediated electrostatic attraction leads to a first-order phase transition similar to that observed in a neutral brush in a poor solvent.[35]

Using the DFT reported in our earlier work,[34] here we study the effects of counterion valence on PEB swelling at various ionic conditions and polyion grafting densities. Because the DFT accounts for the valence of all ionic species explicitly, we expect that it provides a unifying theoretical framework to study counterion-mediated electrostatic correlations and the ionic screening effects. For direct comparison with established results, our calculations are focused on the structure and electrostatic properties of PEBs at conditions where the monovalent and multivalent counterions have the same concentration or ionic strength. After briefly recapitulating the molecular model and theory, we discuss the influence of valence on the microscopic structure of PEBs and the connection of ionic distributions to the electrostatic potential. Next, we present theoretical predictions on the effects of the polyion grafting density and salt concentration on the swelling behavior. A comparison of the theory with experiments is attempted upon gradual replacement of monovalent counterions with multivalent ions at the same ionic strength.

Molecular Model and Theory

As in our previous work,[34,35] we consider a primitive model for highly charged PEB systems (i.e., the polyions are represented by freely jointed chains of charged hard spheres with one end tethered to a planar surface, the counterion and coion are modeled as charged hard spheres with the size identical to a polyion segment, and the solvent is represented by a continuous dielectric medium corresponding to an aqueous environment). We assume that the polyelectrolytes are in a good solvent such that the solvent-mediated attraction between polymer segments can be neglected.

According to the primitive model, the pair interaction potential between two arbitrary charged spheres (i.e., polyion segments or small ions) is given by

$$\beta u_{ij}(r) = \begin{cases} \infty & r < \sigma \\ l_B Z_i Z_j / r & r \geq \sigma \end{cases} \quad (1)$$

In eq 1, r stands for the center-to-center distance between two arbitrary spheres, $\sigma = 0.425$ nm corresponds to the diameter of a hydrated ion, Z_i is the valence of sphere i, and $\beta = (k_B T)^{-1}$ with k_B being the Boltzmann constant and T the absolute temperature. The Bjerrum length is defined as $l_B = \beta e^2/\varepsilon$, where e is the unit charge and ε is the dielectric constant. Throughout this work, we assume $l_B = 0.714$ nm, corresponding to that for liquid water at ambient conditions.

For a tethered chain of freely-jointed hard spheres, the bonding potential $V_b(\mathbf{R})$ is determined from

$$\exp[-\beta V_b(\mathbf{R})] = k\delta(z_1 - \sigma/2)\prod_{i=1}^{M-1}\delta(|\mathbf{r}_{i+1} - \mathbf{r}_i| - \sigma) \quad (2)$$

In eq 2, $\mathbf{R} \equiv (\mathbf{r}_1, \mathbf{r}_2, ..., \mathbf{r}_M)$ is a multidimensional vector that specifies the individual positions of spheres for a polymer with M segments, $\delta(z)$ denotes the one-dimensional Dirac δ function, z_1 represents the perpendicular distance of the tethered segment from the surface, and k is a renormalization constant that is determined from the polyion grafting density.

Except the tethered segments of polyions, all particles are subjected to an external surface energy represented by the hard-wall potential

$$\beta\Psi_i(z) = \begin{cases} \infty & z < \sigma/2 \\ 0 & z \geq \sigma/2 \end{cases} \quad (3)$$

where z denotes the perpendicular distance from the planar surface. We assume that the dielectric constant of the surface is identical to that of water so that the image-charge effect can be neglected.

Within the primitive model, the Helmholtz energy functional can be expressed in terms of an ideal part corresponding to that of an ideal gas of ionic species and polymers free of nonbonded interactions, and an excess accounting for the nonbonded inter- and intramolecular interactions

$$F[\rho_M(\mathbf{R}), \{\rho_\alpha(\mathbf{r})\}] = F^{id}[\rho_M(\mathbf{R}), \{\rho_\alpha(\mathbf{r})\}] + F^{ex}[\rho_M(\mathbf{R}), \{\rho_\alpha(\mathbf{r})\}] \quad (4)$$

where $\rho_M(\mathbf{R})$ stands for a multidimensional density profile of the polyions as a function of configuration $\mathbf{R}$ and $\rho_\alpha(\mathbf{r})$ is the density profiles of small ions.

The Helmholtz energy functional for the ideal part is known exactly as

$$\beta F^{id} = \int d\mathbf{R}\rho_M(\mathbf{R})[\ln \rho_M(\mathbf{R}) - 1] + \beta\int d\mathbf{R}\rho_M(\mathbf{R})V_b(\mathbf{R}) + \sum_{\alpha=+,-}\int d\mathbf{r}\rho_\alpha(\mathbf{r})[\ln \rho_\alpha(\mathbf{r}) - 1] \quad (5)$$

The excess Helmholtz energy functional arises from intermolecular interactions and the correlation effects. For the PEB model considered in this work, it can be further divided into contributions due to the excluded-volume effects, direct Coulombic interactions, and charge/chain correlations.

$$\beta F^{ex} = \int d\mathbf{r}\left\{-n_0 \ln(1-n_3) + \frac{n_1 n_2 - \mathbf{n_{V1}}\mathbf{n_{V2}}}{1-n_3} + \frac{1}{36\pi}\left[n_3 \ln(1-n_3) + \frac{{n_3}^2}{(1-n_3)^2}\right]\frac{({n_3}^2 - 3n_2\mathbf{n_{V2}}\mathbf{n_{V2}})}{{n_3}^3}\right\} +$$
$$\frac{1-M}{M}\int d\mathbf{r}\; n_{0p}(1 - \mathbf{n_{V2p}}\mathbf{n_{V2p}}/{n_{2p}}^2)\ln y(\sigma_p, n_\alpha) + \frac{l_B}{2}\sum_{i,j}\int\int d\mathbf{r}\, d\mathbf{r}'\, \frac{Z_i Z_j \rho_i(\mathbf{r})\rho_j(\mathbf{r}')}{|\mathbf{r} - \mathbf{r}'|} + \quad (6)$$
$$\beta F_{el}^{ex}(\{{\rho_i}^b\}) - \int d\mathbf{r}\sum_i \Delta C_i^{(1)el}[\rho_i(\mathbf{r}) - {\rho_i}^b] - \frac{1}{2}\int\int d\mathbf{r}\, d\mathbf{r}'\sum_{i,j}\Delta C_{ij}^{(2)el}[\rho_i(\mathbf{r}) - {\rho_i}^b][\rho_j(\mathbf{r}') - {\rho_j}^b]$$

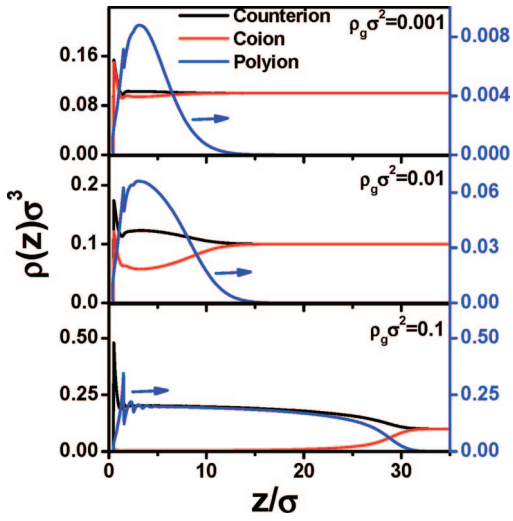

Figure 1. Density profiles of counterions (black), coions (red) (left y-axis), and polyion segments (blue) (right y-axis) in polyelectrolyte brushes at different grafting densities. Here the counterion valence is $Z_+ = 1$; the number of segments per polyion is $M = 50$, the salt concentration in the bulk is $\rho_s\sigma^3 = 0.1$, and the coion valence is $Z_- = -1$. See text for details.

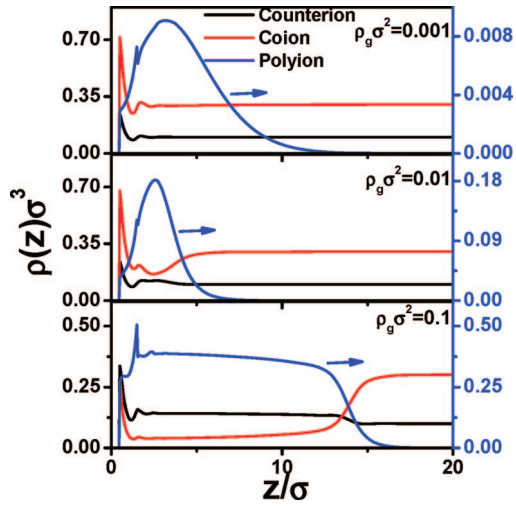

Figure 2. Same as that in Figure 1 but for counterion valence $Z_+ = 3$.

In eq 6, $n_\alpha(\mathbf{r})$, $\alpha = 0$, 1, 2, and 3; V1 and V2 are the scalar- and vector-weighted densities from the fundamental measure theory (FMT);[39] $\Delta C_i^{(1)el}$ and $\Delta Cij^{(2)el}(r)$ are, respectively, the first-order and second-order electrostatic direct correlation functions of charged particles at bulk densities ρ_i^b; $F_{el}^{ex}(\{\rho_i^b\})$ is the corresponding electrostatic Helmholtz energy of the charged particles in the bulk; and $y(\sigma_p,n_\alpha)$ stands for the contact value of the cavity correlation function of the polyion segments.

The first line in eq 6 comes from a modified FMT for hard spheres.[40,41] This term gives a quasi-exact description of the free energy affiliated with the excluded volumes of unbonded polymeric segments and small ions. The second term represents the Helmholtz energy due to the intrachain correlation, which is accounted for by the first-order thermodynamic perturbation theory.[42,43] The third term arises from the direct Coulombic interactions among charged species. Finally, the Helmholtz energy due to the electrostatic correlations (last line in eq 6) is derived from a quadratic functional expansion of the electrostatic free energy,[44,45] where the direct correlation functions of the uniform reference system are obtained from the mean-spherical approximation.[46] The numerical performance of individual terms in eq 2 has been repeatedly calibrated in our previous publications.

Results and Discussion

A. Effect of Grafting Density. In a typical mean-field theory, the ionic distributions are described by the Boltzmann equation that links the charge density exclusively to the mean electrostatic potential. The distribution of polyion segments is described by the Edwards equation for the polymer order parameter. The ionic and polymer densities are coupled only through the mean electrostatic potential. By contrast, the DFT takes into consideration not only the electrostatic interactions between polyions and small ions but also local excluded volume effects and charge correlations.

We first consider the microscopic structure of a PEB in terms of the distribution of polyions and small ions. Figures 1 and 2 present the density profiles of all ionic species in a model PEB at different grafting densities of polyions. For clarity, the density profile of the polyion is affiliated with the right y-axis and those of small ions (i.e., counterions and coions) are with the left y-axis. Two different counterions are presented, with valence $Z_+ = 1$ and 3, respectively. Here the salt concentration in the bulk is fixed at $\rho_s\sigma^3 = 0.1$ (~2.2 M), which corresponds to a condition for "salted brush".[34] Throughout this work, we assume that each polyion segment bears one negative charge (i.e., $Z_p = -1$) identical to that for a coion ($Z_- = -1$) and the number of segments in each polyion chain is fixed at $M = 50$. As discussed in a previous work,[34] an increase of the chain length does not alter the qualitative behavior of PEB swelling.

Figure 1 shows that when the counterions are monovalent, the distribution of polyion segments follows a parabolic profile at low polyion grafting density, resembling that of a neutral brush. The blip near the surface (at $z = 1.5\sigma$) arises from the polyion segments immediately connected to those tethered to the surface. Similar blips can be identified in all other tethered chains and have been confirmed by recent molecular simulations.[26] At low grafting density, the distributions of counterions and coions are little affected by the sparse polyions. Because of the low polyion density, the density profiles of counterions and coions nearly repeat each other, suggesting the condition of local charge neutrality. Accumulation of the ionic species near the surface can be explained by the excluded-volume effect due to the ionic species, similar to that for hard spheres near a hard wall.[41] With the increase of the polyion grafting density, the increase of the brush thickness is evidenced by the extension of the brush rim. The swelling of PEB is accompanied by a drastic depletion of the coions within the brush due to the Donnan effect. The density distributions of small ions outside the brush are nearly uniform, suggesting that the electrostatic neutrality is satisfied beyond the boundary of the PEB. At high grafting density ($\rho_g\sigma^2 = 0.1$), the density profile of polyions oscillates slightly near the surface and maintains more or less uniform throughout the entire region of the extended brush. The slight oscillation of the polyion density can be attributed to the tethering effect.

Qualitatively, the structure of a PEB is little changed by increasing the counterion valence. Figure 2 shows that, similar to that in a monovalent solution, polyions exert no noticeable effect on the distribution of counterions and coions at low grafting density ($\rho_g\sigma^2 = 0.001$). At high grafting density ($\rho_g\sigma^2 = 0.1$), the polyions become more extended, concomitant with the depletion of the coions from the brush. While at low grafting density the configuration of a polyion resembles that of a neutral chain regardless of the counterion valence, the brush thickness

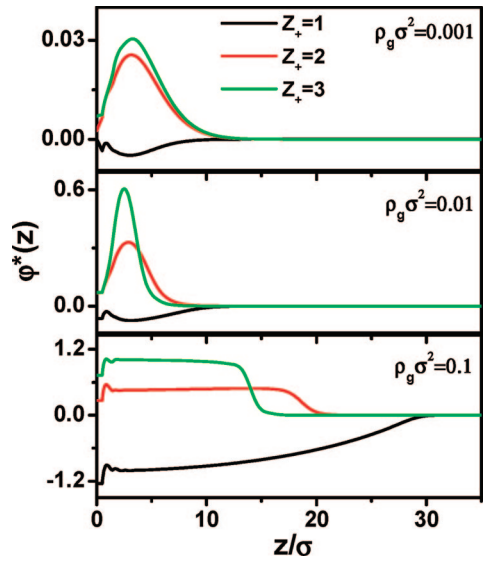

Figure 3. Distributions of the mean electrostatic potentials at different grafting densities of polyions and counterion valences.

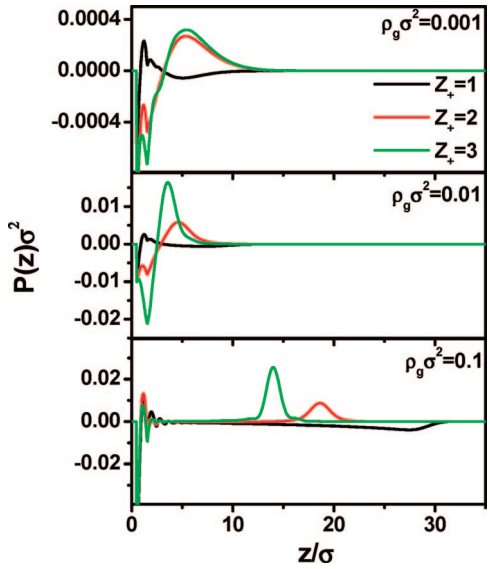

Figure 4. Integrated charge distributions at different grafting densities of polyions and counterion valences.

is noticeably reduced at intermediate grafting density as the valence of counterions increases. Most interestingly, in the presence of multivalent counterions, the density profile of polyion segments recedes as the grafting density increases from the low density limit and reswells at high grafting density. At an intermediate grafting density ($\rho_g\sigma^2 = 0.01$), the brush rim appears approximately at $z = 8\sigma$, much reduced in comparison to $z = 15\sigma$ for $Z_+ = 1$. Because the bare interaction between polyions is purely repulsive according to the primitive model, the reduction of brush thickness can only be explained by the counterion-mediated electrostatic attraction between polyions. The attraction is magnified as the valence of counterions increases.[3,4,8,14]

According to a previous Monte Carlo simulation,[47] electrostatic attraction between like-charged macroions is most significant at an intermediate concentration of counterions. A similar effect can be identified in a polyelectrolyte brush. As more polyelectrolytes are attached to the surface, the effective surface charge density increases and more counterions are present in the brush. Unlike monovalent counterions that play only a screening role on the polyion charges, multivalent counterions introduce stronger electrostatic correlations in ionic distributions and charge inversion of polyions. The counterion-mediated attraction between polyions is responsible for the PEB collapse as the grafting density increases from the low density limit. At sufficiently high grafting density, the strength of electrostatic attraction is reduced because of the elevated concentration of counterions. As a result, the short-range repulsion between polyions and excluded-volume effects of all ionic species compel the reswelling of the PEB at high grafting density. Interestingly, the electrostatic neutrality of the brush is maintained in the presence of multivalent counterions. The charge balance within the brush is also evidenced by the uniform distributions of small ions beyond the brush boundary.

To provide further insights on how the electrostatic correlation affects the PEB structures, we calculate the distribution of mean electrostatic potential inside the PEBs with different valences of counterions. The reduced mean electrostatic potential is calculated from

$$\psi^*(z) \equiv \beta e\psi(z) = 4\pi l_B \int_z^\infty dz'(z - z') \sum_{k=p,+,-} Z_k\rho_k(z') \quad (7)$$

Equation 7 is derived by an integration of the Poisson equation. Figure 3 shows that, for systems with monovalent counterions, the mean electrostatic potential exhibits a negative minimum near the surface and rises monotonically to zero at the brush boundary. The negative potential field is mainly due to the presence of the tethered PEBs. Except at the high grafting density ($\rho_g\sigma^2 = 0.1$), the electrostatic potential vanishes almost everywhere within the brush, which corroborates with the notion that, in presence of monovalent counterions, the structure of a salted brush resembles that of grafted neutral polymers in a good solvent. On the contrary, multivalent counterions overcharge the brush region and induce local charge inversion, which signals the counterion-mediated electrostatic attraction between like-charged polyions. At low grafting density, the electrostatic potential shows a positive Gaussian-like distribution near the surface when the PEB is in contact with a multivalent solution. However, similar distributions are not observed in the density profiles of coions. The drastic difference in the shapes of ionic density profiles and the mean electrostatic potential indicates that, unlike the mean-field predictions, the distribution of ionic species depends not only on the electrostatic potential.

Figure 3 also shows that the magnitude of charge inversion increases with the counterion valence and with the grafting density. At high grafting density, the presence of multivalent counterions makes the mean electrostatic potential nearly constant throughout the brush region. The constant electrostatic potential affirms the uniform density distribution of all charged species within the brush, as shown in Figure 2. Regardless of the counterion valence, the electrostatic potential vanishes at the brush boundary, which reflects preservation of the charge neutrality outside the brush region.

The charge inversion is also manifested in the integrated charge distribution function that describes an overall charge near the surface

$$P(z) = \int_0^z dz' \sum_{k=p,+,-} Z_k\rho_k(z') + \frac{Q}{e} \quad (8)$$

The integrated distribution is related to the mean electrostatic potential by $d\psi^*(z)/dz = -4\pi l_B P(z)$. Since the surfaces in this study are always neutral (i.e., $Q/e = 0$), $P(z)$ includes only contributions from the polyions and small ions. Within contact

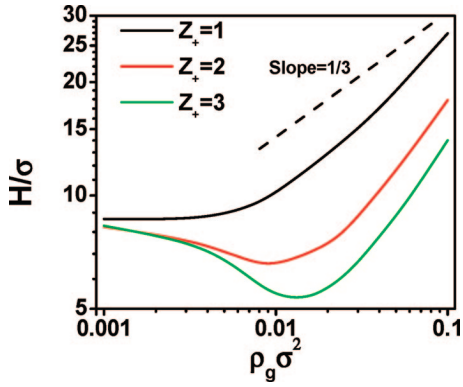

Figure 5. Brush thickness versus the grafting density of polyions at different valences of counterions. The dashed lines highlight the power-law exponents predicted by the scaling laws.

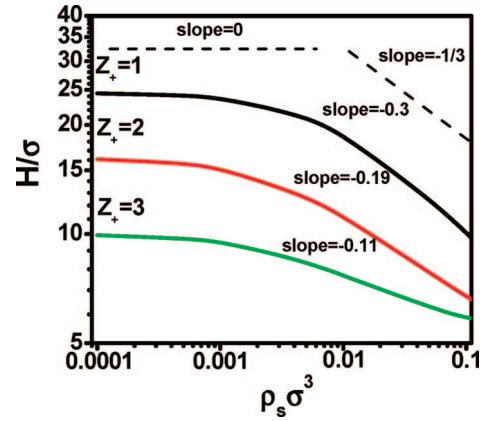

Figure 6. Brush thickness versus the salt concentration for brushes with counterions of different valences. In all cases, the grafting density is $\rho_g\sigma^2 = 0.01$. The dashed lines are predictions from the scaling laws for the "salted" and "osmotic" brushes.

($z \leq 0.5\sigma$), the negative minimum of $P(z)$ in Figure 4 is solely determined by the tethering polyion segments. The kinks near the surface (within $z \leq 1.5\sigma$) are due to the polyion segments immediately connected to tethered ones and coupled small ions. For systems with monovalent counterions, the integrated charge distribution is negative throughout the entire brush region and exhibits a minimum near the brush end, suggesting accumulation of negatively charged polyions. The magnitude of the negative minimum also increases with the brush grafting density. When the counterions are multivalent, the charge inversion occurs at very low grafting density. The integrated charge distribution shows a positive Gaussian-like distribution near the brush end, reflecting the overcharging from the multivalent counterions. The position of the maximum value shifts corresponds to the brush thickness, and the magnitude increases with the counterion valence and grafting density.

From the density profiles of polyion segments, we can readily calculate the brush thickness, which is defined by the first moment of the density profile of polyion segments:

$$H = 2\int_0^\infty z\rho_p(z)\,dz \Big/ \int_0^\infty \rho_p(z)\,dz \qquad (9)$$

Figure 5 shows that, as well-documented, the brush thickness varies little at low grafting density. In this case, the electrostatic repulsion between polyions is effectively screened by the abundance of salt ions from the bulk solution. As for a neutral brush, the primary driving force for brush swelling is the excluded-volume effect and short-range electrostatic repulsion. The short-range repulsion is most prominent when the overall packing density of all species is sufficiently high (i.e., beyond the intermolecular correlation length). In the presence of monovalent counterions, the brush exhibits a quasi-power-law expansion with the increase of the grafting density.[27,48,49] The situation becomes more complicated in the presence of multivalent counterions. The PEB first collapses with the increase of the grafting density because of the counterion-mediated electrostatic correlations. At sufficiently high grafting density, the PEB reswells because of the short-range repulsions.

Figure 5 shows a minimum brush thickness at $\rho_g\sigma^2 = 0.01$ for divalent counterions and at $\rho_g\sigma^2 = 0.015$ for trivalent counterions. The nonmonotonic swelling behavior can be explained by a counterbalance of electrostatic attraction and excluded-volume effects. The collapse of a PEB is most dramatic in the presence of trivalent counterions. Interestingly, at high grafting density, the slope of PEB swelling is essentially invariant with the counterion valence, implying a common driving force in this regime (i.e., the brush reswells because of the short-range repulsion). While the brush thickness is a crossover function of the grafting density instead of the pure power law, the power-law dependence of the brush thickness on the grafting density is fairly comparable to those from the scaling analyses and experiments at high grafting density ($H \propto \rho_g^{1/3}$).[27,48,49] Nevertheless, the overall brush thickness remains sensitive to the counterion valence, implying the different mechanism of brush swelling from that of a neutral brush.

B. Effect of Salt Concentration. According to the scaling analysis and mean-field theory predictions,[27,28,50] a PEB undergoes a sharp transition from the "osmotic brush" regime to the "salted brush regime" in response to the continuous increase of the salt concentration. In the "osmotic brush" regime, the brush thickness scales as $H \propto \rho_s^0$ and in the "salted brush" regime as $H \propto \rho_s^{-1/3}$. For a PEB in contact with monovalent counterions, the mean-field predictions have been extensively tested with experiments[48,49,51] and agree with the DFT as reported in our earlier work.[34] Because both the scaling analysis and mean-field theories do not explicitly consider the ionic valence, it remains an open question whether the same scaling relations are valid for multivalent counterions. In Figure 6, we compare the dependence of the brush thickness on the salt concentration in solutions containing counterions of different valences. In these calculations, the grafting density is fixed at $\rho_g\sigma^2 = 0.01$, with the salt concentration spanning 4 orders of magnitude (i.e., from $\rho_s\sigma^3 = 0.0001$ to 0.1). In all cases, we can identify the "osmotic" and "salted" brush regimes according to the brush thickness. In a monovalent solution, the "osmotic brush" regime corresponds to a range of salt concentration where the brush thickness is essentially constant. The "salted brush" regime corresponds to a range of salt concentration where the brush thickness follows the scaling relation $H \propto \rho_s^{-0.3}$. As reported in a previous work,[34] the DFT predicts the scaling relations in both regimes in good agreement with those from the scaling analysis and mean-field theories.[27,28,50] In between these two regions, we find a smooth transition instead of a first-order transition predicted by mean-field theories.

Figure 6 shows that, in the presence of multivalent counterions, a PEB can be divided into an "osmotic brush" regime and a "salted brush" regime similar to those that appeared in a solution with only monovalent counterions. Apparently, the osmotic brush regime shrinks as the counterion valence increases. Moreover, the exponent in the power-law relations varies noticeably with the counterion valence. In the salted brush regime, we find that the slope is -0.19 for $Z_+ = 2$ and -0.11

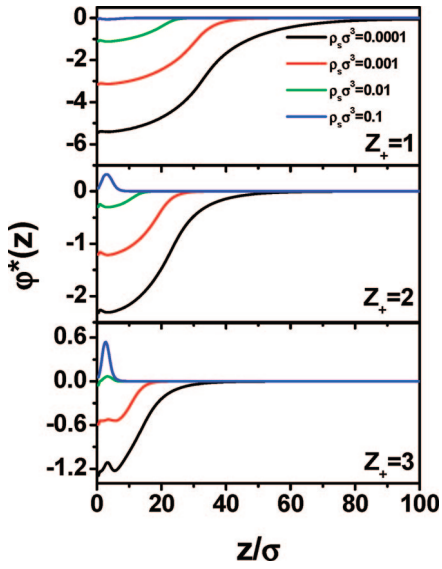

Figure 7. Distribution of the mean electrostatic potential in polyelectrolyte brushes at different salt concentrations. All parameters are the same as those used in Figure 6.

for $Z_+ = 3$, in comparison to -0.3 for $Z_+ = 1$. Qualitatively, all trends predicted by DFT agree well with experiments.[52] For example, in a recent experiment on polystyrene sulfonic acid spherical brush,[52] Guo and Ballauff found that no osmotic regime can be truly identified over an appreciable range of salt concentration in the presence of multivalent counterions (Mg^{2+}). Instead, the brush collapse starts at very low salt concentration. Although a scaling relation can be identified for the brush collapse, it is less pronounced than that of "salted brush" regime in the case of monovalent counterions. At a moderate grafting density, the primary driving force of the brush swelling is the electrostatic repulsion among like-charged polyions. In comparison to monovalent counterions at the same salt concentration, multivalent counterions provide more effective neutralization of the polyions so that the brush collapses at much lower salt concentration. Approximately, the power-law exponent is proportional to the ionic valence.

Figure 7 shows the distributions of the mean electrostatic potential for those systems considered in Figure 6. In the presence of monovalent counterions, the electrostatic potential is highly negative and extends far beyond the brush boundary at low salt concentration. With the increase of the salt concentration, both the magnitude and range of the electrostatic potential shrink dramatically. At high salt concentration ($\rho_s\sigma^3 = 0.1$), the mean electrostatic potential is nearly zero everywhere, suggesting a complete screening of the electrostatic charge as discussed earlier. With the presence of multivalent counterions, the electrostatic potential is less negative because of the more effective screening. Charge inversion appears at sufficiently high salt concentrations, where the monotonic negative potential turns into a Gaussian-like positive potential near the surface. The charge inversion occurs at lower salt concentration as the counterion valence increases from divalent to trivalent.

C. Effect of Counterion Exchange. As demonstrated in recent experiments,[31,32] the effect of counterion valence on the brush thickness can be studied by immersing a PEB into a solution containing a mixture of counterions of different valences. At a fixed ionic strength, successive replacement of monovalent counterions with multivalent ones may also lead to the brush collapse. To investigate such an effect, we

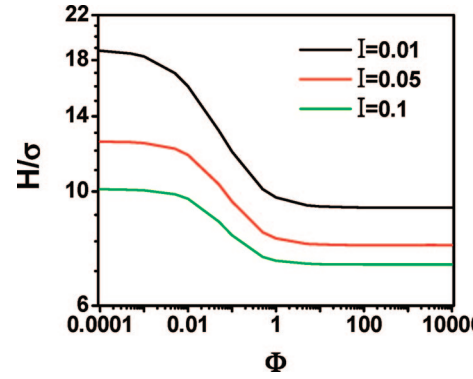

Figure 8. Brush thickness in the presence of a mixture of monovalent and trivalent counterions at fixed ionic strength. Here, the grafting density is $\rho_g\sigma^2 = 0.01$.

calculated the microscopic structure and thickness of a PEB in a mixture of monovalent and trivalent counterions at different ratios of the counterion concentrations ($\Phi = \rho_s^{3+}/\rho_s^{+}$). As before, the grafting density of PEB is fixed at $\rho_g\sigma^2 = 0.01$. At a given ionic strength, $I = 1/2\sum_i Z_i^2\rho_{s,i}\sigma^3$, where i represents coions and different counterions, the concentrations of small ions can be solved from the concentration ratio Φ and the neutralization condition.

Figure 8 shows the brush thicknesses at three different overall ion strengths: $I = 0.01$, 0.05, and 0.1. At low concentration ratio, the brush thickness is more or less constant, in good agreement with experimental results. In this case, the multivalent counterions are primarily distributed in the bulk because of the translational entropy and the brush thickness is close to that with only monovalent counterions. A smooth reduction of the brush thickness is predicted as the concentration ratio increases from $\Phi = 0.01$ to 1. Approximately, the range of concentration ratio is independent of the ionic strengths. As observed in experiments, in this range the brush thickness shows a quasi-power-law dependence on Φ. The power-law exponent shows a slight decrease with the increase of ion strength, which is -0.12 for $I = 0.01$, -0.09 for $I = 0.05$, and -0.07 for $I = 0.1$. At high concentration ratio ($\Phi > 1$), the charges of polyions are fully compensated by the trivalent counterions. In that case, a further increase of the concentration ratio has little effect on the brush thickness and the ionic distributions.

Figure 9 presents the density profiles of the polyion segments and salt ions for the brushes at different counterion concentration ratios with a fixed ionic strength ($I = 0.1$). All parameters are the same as those considered in Figure 8. At low concentration ratio, almost no trivalent counterions enter the brush region so that the density distributions of polyion, monovalent counterions, and coions are essentially the same as those of $\rho_g\sigma^2 = 0.01$ in Figure 1. As before, accumulation of monovalent ions near the surface is primarily due to the excluded-volume effect. With the gradual replacement of monovalent counterions with trivalent ones, the brush tail recedes accompanied by accumulation of trivalent ions near the surface. Unlike monovalent counterions that accumulate near the surface, the trivalent ions distribute approximately in superposition with the polyions, suggesting a stronger electrostatic association. At high ratio of the trivalent-to-monovalent counterion concentrations ($\Phi > 1$), the density profiles of polyions and trivalent counterions are little affected by the further decrease of the monovalent counterion density. In that case, the brush thickness becomes invariant to Φ as shown in Figure 8.

Figure 10 shows the distributions of mean electrostatic potential for the same systems considered in Figure 9. At low

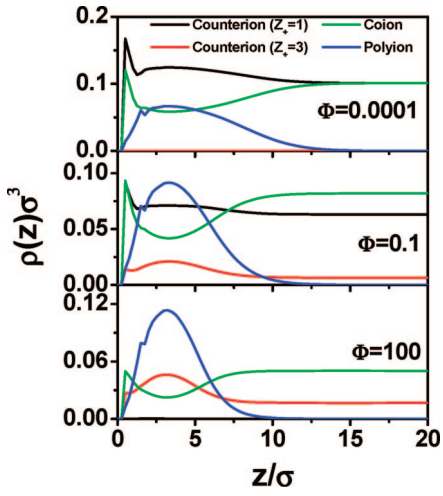

Figure 9. Density profiles of monovalent counterions, trivalent counterions, coions, and polyions in polyelectrolyte brushes at different ratios of counterion concentrations. Here, the reduced ionic strength is $I = 0.1$. All parameters are the same as those used in Figure 8.

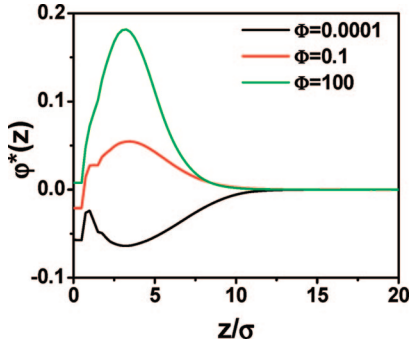

Figure 10. Distributions of the mean electrostatic potentials in polyelectrolyte brushes at different ratios of counterion concentrations. All parameters are the same as those used in Figure 9.

concentration ratio, the potential is exclusively negative in the brush region and, after a weak maximum due to depletion of the polyions at the surface, monotonically approaches zero at the brush boundary. Addition of trivalent counterions ($\Phi = 0.1$) results in variation of the electrostatic potential in the entire brush region. In particular, the electrostatic potential becomes positive except right at the surface. At $\Phi = 100$, the mean electrostatic potential is totally positive and shows a Gaussian-like distribution. Because the charge neutrality is maintained beyond the brush boundary, it appears that the charge inversion within the brush region has little effect on the ionic distribution outside the brush.

Conclusions

We have demonstrated that the swelling behavior of a polyelectrolyte brush (PEB) is highly sensitive to the counterion valence and salt concentration. While in a monovalent solution the brush thickness increases monotonically with the grafting density, multivalent counterions may induce the brush collapse at an intermediate grafting density and reswelling at high grafting density. At high salt concentration ("salted brush"), the brush collapses because of the attraction between like-charged polyions. The correlation effect of ionic distributions is also manifested in the overcharging of polyions in the presence of divalent or trivalent counterions. At an intermediate grafting density, the brush collapses when the counterion-mediated attraction becomes more significant than the excluded-volume effect. At high grafting densities, however, the brush reswells because of the reduction of counterion-mediated attraction and magnified excluded-volume effects. While the brush thickness is noticeably reduced in the presence of multivalent counterions, it shows similar scaling behavior at high grafting density independent of the counterion valence.

Although a polyelectrolyte brush shrinks with the increase of counterion valence at the same concentration or ionic strength, different brush regimes can still be identified at the same range of salt concentrations. In the "osmotic brush" regime, the brush thickness is insensitive to the salt concentration regardless of the counterion valence. In the "salted brush" regime, the brush thickness follows a power-law scaling relation to the salt concentration. The absolute value of the power-law exponent is almost inversely proportional to the counterion valence. We also examined the brush collapse in the presence of a mixture of trivalent and monovalent counterions. At the fixed ionic strength, replacement of monovalent counterions by trivalent ones leads to brush collapse. The transitions to the collapse state happen approximately at the same range of concentration ratios for all ionic strengths.

Finally, we demonstrated that, unlike typical mean-field predictions, the ionic distributions within a brush depend not only on the mean electrostatic potential but also on the segment-level pair interactions and correlation effects. In particular, the density profiles of ionic species can be qualitatively different from predictions of the conventional Boltzmann in the presence of multivalent counterions.

Acknowledgment. For financial support, we are grateful to the U.S. Department of Energy (DE-FG02-06ER46296). This research used computer time allocation from the National Energy Research Scientific Computing Center (NERSC), which is supported by the Office of Science of the U.S. Department of Energy under Contract No. DE-AC03-76SF00098.

References and Notes

(1) Israelachvili, J. *Intermolecular and Surface Forces*; Academic Press: London, 1985.
(2) Gelbart, W. M.; Bruinsma, R. F.; Pincus, P. A.; Parsegian, V. A. *Phys. Today* **2000**, *53*, 38.
(3) Butler, J. C.; Angelini, T.; Tang, J. X.; Wong, G. C. L. *Phys. Rev. Lett.* **2003**, *91*, 028301.
(4) Angelini, T. E.; Liang, H.; Wriggers, W.; Wong, G. C. L. *Proc. Natl. Acad. Sci. U.S.A.* **2003**, *100*, 8634.
(5) Bloomfield, V. A. *Curr. Opin. Struct. Biol.* **1996**, *6*, 334.
(6) Tang, J. X.; Janmey, P. A. *J. Biol. Chem.* **1996**, *271*, 8556.
(7) Podgornik, R.; Rau, D. C.; Parsegian, V. A. *Biophys. J.* **1994**, *66*, 962.
(8) Gronbech-Jensen, N.; Mashl, R. J.; Bruinsma, R. F.; Gelbart, W. M. *Phys. Rev. Lett.* **1997**, *78*, 2477.
(9) Sarraguca, J. M. G.; Pais, A. *Phys. Chem. Chem. Phys.* **2006**, *8*, 4233.
(10) Zribi, O. V.; Kyung, H.; Golestanian, R.; Liverpool, T. B.; Wong, G. C. L. *Phys. Rev. E* **2006**, 73.
(11) Lee, K. C.; Borukhov, I.; Gelbart, W. M.; Liu, A. J.; Stevens, M. J. *Phys. Rev. Lett.* **2004**, *93*, 128101.
(12) Naji, A.; Netz, R. R. *Eur. Phys. J. E* **2004**, *13*, 43.
(13) Liu, S.; Ghosh, K.; Muthukumar, M. *J. Chem. Phys.* **2003**, *119*, 1813.
(14) Ha, B. Y.; Liu, A. J. *Phys. Rev. Lett.* **1997**, *79*, 1289.
(15) Pincus, P. A.; Safran, S. A. *Europhys. Lett.* **1998**, *42*, 103.
(16) Podgornik, R.; Parsegian, V. A. *Phys. Rev. Lett.* **1998**, *80*, 1560.
(17) Shklovskii, B. I. *Phys. Rev. Lett.* **1999**, *82*, 3268.
(18) Kornyshev, A. A.; Leikin, S. *Phys. Rev. Lett.* **1999**, *82*, 4138.
(19) Rouzina, I.; Bloomfield, V. A. *J. Phys. Chem.* **1996**, *100*, 9977.
(20) Golestanian, R.; Kardar, M.; Liverpool, T. B. *Phys. Rev. Lett.* **1999**, *82*, 4456.
(21) Guenoun, P.; Argillier, J. F.; Tirrell, M. *C. R. Acad. Sci., Ser. IV: Phys., Astrophys.* **2000**, *1*, 1163.
(22) Ruhe, J.; Ballauff, M.; Biesalski, M.; et al. *Adv. Polym. Sci.* **2004**, *165*, 79.

(23) Ballauff, M.; Borisov, O. *Curr. Opin. Colloid Interface Sci.* **2006**, *11*, 316.
(24) Ahrens, H.; Forster, S.; Helm, C. A. *Macromolecules* **1997**, *30*, 8447.
(25) Romet-Lemonne, G.; Daillant, J.; Guenoun, P.; Yang, J.; Mays, J. W. *Phys. Rev. Lett.* **2004**, *93*, 148301.
(26) Kumar, N. A.; Seidel, C. *Macromolecules* **2005**, *38*, 9341.
(27) Pincus, P. *Macromolecules* **1991**, *24*, 2912.
(28) Borisov, O. V.; Birshtein, T. M.; Zhulina, E. B. *J. Phys. II* **1991**, *1*, 521.
(29) Gong, P.; Genzer, J.; Szleifer, I. *Phys. Rev. Lett.* **2007**, 98.
(30) Santangelo, C. D.; Lau, A. W. C. *Eur. Phys. J. E* **2004**, *13*, 335.
(31) Mei, Y.; Lauterbach, K.; Hoffmann, M.; Borisov, O. V.; Ballauff, M.; Jusufi, A. *Phys. Rev. Lett.* **2006**, *97*, 158301.
(32) Plamper, F. A.; Walther, A.; Muller, A. H. E.; Ballauff, M. *Nano Lett.* **2007**, *7*, 167.
(33) Fazli, H.; Golestanian, R.; Hansen, P. L.; Kolahchi, M. R. *Europhys. Lett.* **2006**, *73*, 429.
(34) Jiang, T.; Li, Z. D.; Wu, J. Z. *Macromolecules* **2007**, *40*, 334.
(35) Jiang, T.; Wu, J. Z. Submitted for publication, *J. Chem. Phys*., **2008**.
(36) Wang, Q. *Macromolecules* **2005**, *38*, 8911.
(37) Li, Z. D.; Wu, J. Z. *J. Phys. Chem. B* **2006**, *110*, 7473.
(38) Li, Z. D.; Wu, J. Z. *Phys. Rev. Lett.* **2006**, *96*, 048302.
(39) Rosenfeld, Y. *Phys. Rev. Lett.* **1989**, *63*, 980.
(40) Roth, R.; Evans, R.; Lang, A.; Kahl, G. *J. Phys.: Condens. Matter* **2002**, *14*, 12063.
(41) Yu, Y. X.; Wu, J. Z. *J. Chem. Phys.* **2002**, *117*, 10156.
(42) Li, Z. D.; Wu, J. Z. *Phys. Rev. Lett.* **2006**, *96*, 048302.
(43) Yu, Y. X.; Wu, J. Z. *J. Chem. Phys.* **2002**, *117*, 2368.
(44) Yu, Y. X.; Wu, J. Z.; Gao, G. H. *J. Chem. Phys.* **2004**, *120*, 7223.
(45) Li, Z. D.; Wu, J. Z. *Phys. Rev. E* **2004**, *70*, 031109.
(46) Blum, L. *Mol. Phys.* **1975**, *30*, 1529.
(47) Wu, J. Z.; Bratko, D.; Prausnitz, J. M. *Proc. Natl. Acad. Sci. U.S.A.* **1998**, *95*, 15169.
(48) Balastre, M.; Li, F.; Schorr, P.; Yang, J. C.; Mays, J. W.; Tirrell, M. V. *Macromolecules* **2002**, *35*, 9480.
(49) Tamashiro, M. N.; Hernandez-Zapata, E.; Schorr, P. A.; Balastre, M.; Tirrell, M.; Pincus, P. *J. Chem. Phys.* **2001**, *115*, 1960.
(50) Zhulina, E. B.; Borisov, O. V.; Birshtein, T. M. *J. Phys. II* **1992**, *2*, 63.
(51) Li, F.; Balastre, M.; Schorr, P.; Argillier, J. F.; Yang, J. C.; Mays, J. W.; Tirrell, M. *Langmuir* **2006**, *22*, 4084.
(52) Guo, X.; Ballauff, M. *Phys. Rev. E* **2001**, 6405.

JP801911A